ACS Photonics

Article

pubs.acs.org/journal/apchd5

Electron Energy-Loss Spectroscopy of Multipolar Edge and Cavity Modes in Silver Nanosquares

Edson P. Bellido,[†] Alejandro Manjavacas,[‡] Yue Zhang,[¶] Yang Cao,[¶] Peter Nordlander,*[,¶] and Gianluigi A. Botton*[,†]

[†]Department of Materials Science and Engineering, McMaster University, 1280 Main Street West, Hamilton, Ontario L8S 4L7, Canada

[‡]Department of Physics and Astronomy, University of New Mexico, Albuquerque, New Mexico 87131, United States

[¶]Department of Physics and Astronomy and Laboratory for Nanophotonics, Rice University, 6100 South Main Street, MS 61, Houston, Texas 77005, United States

Supporting Information

ABSTRACT: The characterization of surface plasmon resonances supported by metallic nanostructures requires high spatial and energy resolution. In the past few years, electron energy loss spectroscopy (EELS) has emerged as a very powerful tool to accomplish this task. In this work, we demonstrate the power of this technique for probing and imaging resonances of metallic nanostructures by analyzing the plasmonic response of silver nanosquares of sizes ranging from 230 nm up to 1 μm. Because of the relatively large size of these structures, we find that, despite their simple geometry, these systems can support a large variety of multipolar modes, which can only be detected and imaged thanks to the high spatial and energy resolution achieved by pushing EELS to its limits. The experimental results are supported by rigorous theoretical calculations that allow a detailed interpretation of the EELS measurements. In particular, we were able to map, with high level of detail, edge and high-order cavity modes. Furthermore, by calculating the scattering cross-section of these nanostructures, we confirm that most of the observed modes are dark and thus remain hidden in optical measurements, thus demonstrating the power of EELS as a unique tool for probing and imaging a large range and variety of plasmonic resonances of metallic nanostructures.

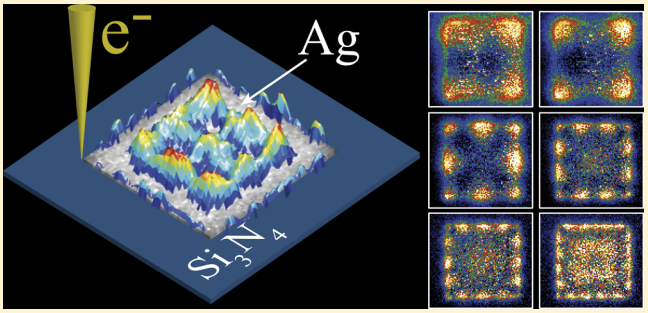

KEYWORDS: *electron energy loss spectroscopy, surface plasmons, edge modes, cavity modes, local density of states, silver nanosquares.*

Metallic nanostructures support collective oscillations of the conduction electrons, commonly known as surface plasmons,[1] which can be exploited to manipulate light at the nanometer scale.[2] The plasmonic response of metallic nanostructures is frequently characterized using different far- and near-field optical techniques.[3] However, although these techniques provide relevant information on the spectral response of the nanostructures, their spatial resolution is limited to some tens of nanometers.[4,5] In this context, electron energy loss spectroscopy (EELS)[6] performed in a scanning transmission electron microscope (STEM), has emerged as a unique tool to study the local optical response of metallic nanostructures,[7] capable of combining an unprecedented spatial resolution[8−15] with the ability to probe bright as well as dark plasmonic modes.[16−21] Furthermore, the use of gun monochromators for STEM-EELS acquisition, together with the utilization of deconvolution techniques for postprocessing, has significantly increased the energy resolution of this technique. The range of measurable energy losses, which was previously limited to the visible range or higher energies, now extends down to the mid-infrared region of the electromagnetic spectrum.[22] This improvement has resulted in an extension of the range of systems that can be studied using EELS to include, for instance, nanostructures with large dimensions or those presenting very closely spaced modes in the energy or the spatial domain, clusters, arrays of nanoparticles, or materials with infrared plasmon resonances,[23] while maintaining, at the same time, its extraordinary high spatial resolution.

In this contribution, we use EELS to study the optical response of silver squares of several lateral sizes ranging from 230 nm up to 1 μm. Despite the simplicity of their shape,[24] we find that, because of their relatively large size, these nanostructures support a collection of multipolar edge and cavity plasmon resonances with energies in the interval from 2.36 down to 0.33 eV. We take advantage of the high energy and spatial resolution of this technique to study the character of these modes, most of which, due to their low excitation

Received: October 16, 2015
Published: February 9, 2016

DOI: 10.1021/acsphotonics.5b00594
ACS Photonics 2016, 3, 428−433

probability, low resonance energy, or the fine spatial features, have not been previously mapped. The experimental results are well supported by rigorous theoretical modeling. Furthermore, by comparing electron energy loss (EEL) spectra with the scattering cross-section of the nanostructures under study, we show that most of the observed plasmonic modes cannot be detected in optical measurements. These results not only emphasize the well-established versatility of this technique for the study of plasmonic resonances but show that simple structures can exhibit a rich variety of resonances well suited to test theoretical models and challenge the limits of experimental techniques.

EELS MEASUREMENTS

The experimental setup and the system under study are sketched in Figure 1a. We study silver nanosquares with a lateral size L and 40 nm of thickness fabricated using electron beam lithography directly on a 50 nm thick silicon nitride transmission electron microscope (TEM) grid. We employ a JSM-7000F scanning electron microscope (SEM) equipped with a nano pattern generation system (NPGS).[22] Figure 1b shows annular dark-field (ADF) images of two of the fabricated nanosquares with L = 230 nm and L = 430 nm. We study the plasmonic response of these systems by measuring their EEL spectra in an STEM−TEM system (Titan 80−300) equipped with a gun monochromator. As shown in Figure 1a, we use a 80 keV electron beam (with a beam current of 1 nA), which is focused on the sample and scanned over the region of interest. After interacting with the silver nanosquare and exciting its surface plasmons, we collect the transmitted electrons simultaneously in an energy loss spectrometer (Gatan Imaging Filter, Tridiem model 865) and in an ADF detector. We record the loss spectra using a 2048 × 128 pixel CCD camera with a dispersion of 10 meV per channel, 8× binning in the nonenergy-dispersive direction, and an exposure time of 1 ms per spectrum. To improve the energy resolution of the spectral images, we apply the Richardson−Lucy algorithm, obtaining effective energy resolutions down to 50 meV measured from the full width at half-maximum of the zero loss peak.[22] We acquire the spectral images using electron beam step sizes as small as 4 nm.

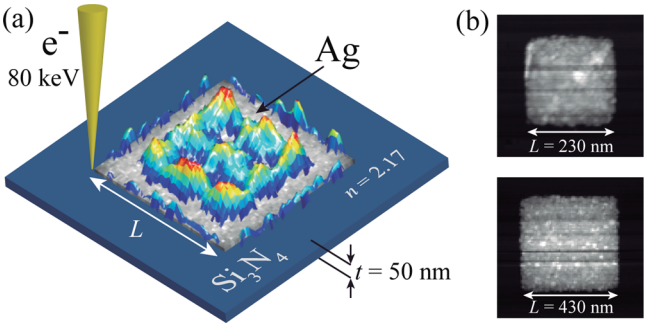

Figure 1. Description of the experimental setup and the system under study. (a) We consider a silver nanosquare of lateral size L and 40 nm of thickness, fabricated on a silicon nitride membrane of thickness t = 50 nm. We use an 80 keV electron beam to excite the different plasmon resonances of this system. (b) Annular dark-field images of two of the silver nanosquares considered in this work.

Figure 2a shows the EEL spectra of silver nanosquares of different lateral sizes L measured using electron beams passing close to the edge of these systems (red-shadowed area in the inset). These spectra show a collection of different plasmon modes. As the size of the square increases, the modes shift to lower energies and higher-order modes become visible. Interestingly, the red-shift occurs at different rates for different modes. This can be noticed by looking at the energy difference between modes 1 and 2, which clearly decreases with increasing size. Remarkably, we are able to resolve these two peaks even for the nanosquare with L = 1 μm, for which the energy difference is only 90 meV. We determine the nature of these plasmon modes from the corresponding EEL maps, which are plotted in Figure 2c for the case of a nanosquare with L = 850 nm (EEL maps for nanosquares of other lateral sizes L can be found in Figures 4c,d and in Figure S1 of the Supporting Information). We obtain these maps by integrating over an energy window of ±30 meV around the corresponding resonance peaks. As seen in Figure 2c we are able to clearly identify six different modes. The EEL probability of the first four modes is concentrated at the edge of the nanostructure. For that reason, we label them as edge modes, each of them having a different multipolar character determined by the number of nodes of the EEL probability along the edge: mode 1 has no node and thus corresponds to a dipolar pattern, mode 2 has one node as expected from a quadrupolar distribution, while modes 3, 4, and 5 have two, three, and four as they correspond to the next multipolar orders, respectively. Similar

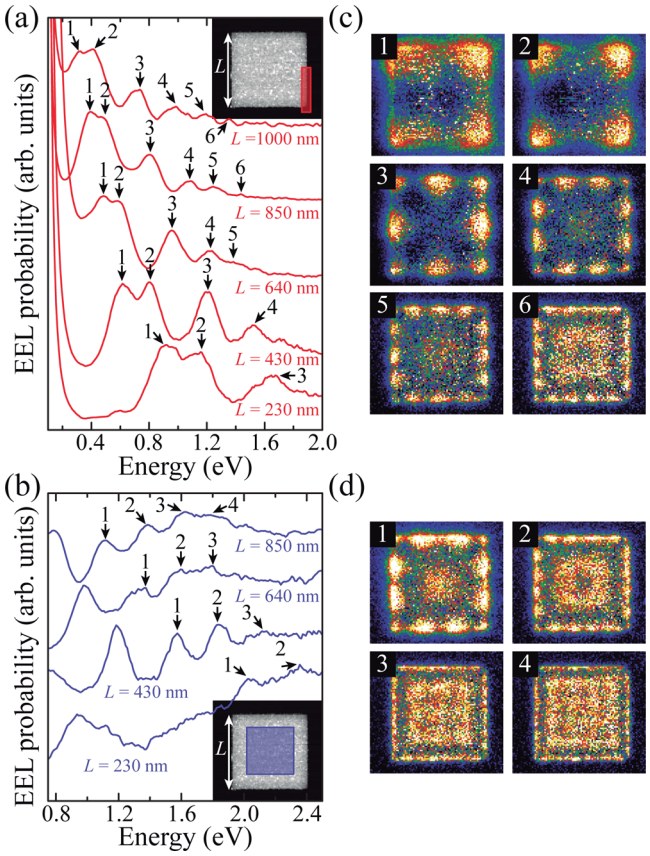

Figure 2. Edge and cavity plasmon modes of silver nanosquares. EEL spectra measured at the edge (a) and at the center (b) (see insets) of silver nanosquares with different lateral sizes L. EEL maps for the L = 850 nm nanosquare corresponding to the edge (c) and cavity (d) plasmon modes shown in (a) and (b), respectively. (EEL maps for nanosquares of other lateral sizes L can be found in the Figure S1 of the Supporting Information).

DOI: 10.1021/acsphotonics.5b00594
ACS Photonics 2016, 3, 428−433

modes have been observed in the EEL maps of nanodisks,[25] nanotriangles,[26] nanocubes,[27] and nanostrips.[28] As the number of nodes increases, the EEL maps start to display some probability in the central region of the nanosquare. This can be noticed for mode 5, whose EEL probability map shows a circular spot at the center, although it is more evident for mode 6. In this case, because of the large number of nodes, the EEL probability along the edge becomes almost constant and a square pattern becomes visible at the center of the nanostructure.

We refer to the modes displaying a strong EEL probability at the center of the nanostructure as cavity modes because they resemble the three-dimensional plasmon modes present in ring-shaped cavities.[29] Similar modes, also referred as breathing modes, have been observed in nanodisks.[25] As expected from their EEL probability maps, these modes are more efficiently excited when the electron beam passes through the center of the nanosquares. This is the case of the EEL spectra shown in Figure 2b, which are obtained by integrating the EEL signal acquired within the blue-shadowed area shown in the inset. As in Figure 2a, we observe a collection of different modes that shift to lower energies as the size of the square increases. We investigate the character of these modes by analyzing their associated EEL probability maps obtained by integrating the signal over a ±60 meV energy window centered at the peak. We plot these maps in Figure 2d for the four plasmon resonances of the L = 850 nm nanosquare. As expected, all modes have a significant EEL probability at the center (see the movie provided in the Supporting Information). We can exploit the analogy of this system with a two-dimensional cavity and label these resonances using a pair of numbers (n, m) corresponding to the number of antinodes that the mode displays along the two axes of the square. Using this notation, the mode 1 in Figure 2b, which displays a spot at the center, corresponds to the (1, 1) mode of the nanocavity. Mode 2 is then identified as the superposition of modes (2, 1) and (1, 2), which, because of the symmetry of the square geometry, are degenerate and therefore are excited simultaneously in our measurements. Exactly the same happens with mode 3, which results from the superposition of modes (3, 1) and (1, 3). Interestingly, modes with $n = m$ and $n > 1$, such as mode (2, 2), cannot be clearly identified from the spectra showed in Figure 2b. However, as shown in Figure 3, this mode becomes visible in the EEL spectrum if instead of integrating the signal of the whole central region (blue-shadowed area in the lower inset of Figure 3), we integrate only the part acquired at the corners of that region (green-shadowed area in the lower inset of Figure 3), where we expect to find the antinodes of the (2, 2) mode. This is clearly confirmed by the analysis of the corresponding EEL maps, which are also plotted as insets in Figure 3. Mode 4, which appears as a broad resonance in the spectrum, can be identified from the corresponding EEL map as the superposition of modes (4, 1) and (1, 4). In contrast, modes (2, 3), (3, 2), and (3, 3) do not appear in the spectrum. These modes, as was the case for mode (2, 2), have a smaller EEL probability compared with modes (n, 1) when the signal from the whole central region is integrated and are therefore obscured by modes (4, 1) and (1, 4). It is worth emphasizing that the high energy resolution achieved due to the reduction on the tails of the zero loss peak, and the relatively high beam currents employed, are the necessary conditions that allow the study of these high-order modes, which have not been previously mapped in such detail.

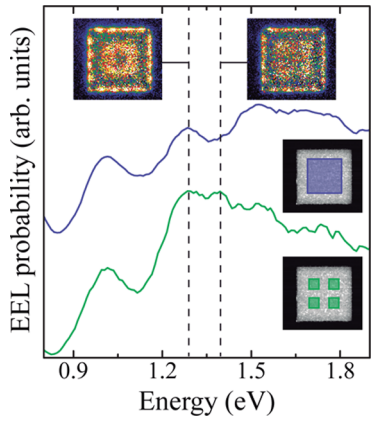

Figure 3. EEL spectra for the silver nanosquare with L = 850 nm obtained from the integration of the EEL signal acquired at two different regions of the nanosquare (blue- and green-shadowed areas of the lower insets). The upper insets show the EEL probability maps corresponding to the energies indicated by the dashed lines.

THEORETICAL SIMULATIONS

To complete our analysis of the multipolar edge and cavity plasmon modes, and to obtain a deeper understanding of the plasmonic response of these nanostructures, we compare our EELS measurements with theoretical simulations based on the rigorous solution of Maxwell's equations using a recently developed finite-difference time-domain (FDTD) EELS solver.[30] Parts a and b of Figure 4 show the comparison between the experimental and the simulated EEL spectra of silver nanosquares with L = 230 nm and L = 430 nm for electron beams passing through different positions. More specifically, we measure the experimental spectra by integrating over the shadowed areas shown in the insets, which are color coded (red for the corner, green for the edge center, blue for 1/4 of the edge, and yellow for the central part of the nanosquare). The same integration area is also used for the simulated spectra, which are calculated using electron trajectories passing through the same areas of the nanostrucure. The agreement between the measured and simulated EEL spectra is very good. We attribute the small discrepancies in the peak position to geometrical defects on the fabricated structures as compared with the perfect shapes used in the simulations. Another possible source of discrepancy are the differences between the values of the thickness t and refractive index n of the substrate (see Figure 1a) used on the simulation and the actual experimental values. A change on those magnitudes can shift the position of the resonances, as shown in Figure S2 of the Supporting Information. Similarly, we attribute the differences on the peak widths to the polycrystalline character of the fabricated nanostructures, which results in broader resonances when compared with the simulations. We also compare the measured EEL probability maps with theoretical simulations of the local density of photonic states (LDOS). More specifically, we consider the component of the LDOS parallel to the electron trajectory calculated on a plane parallel to the silver nanosquares and situated 5 nm above them (cf. Figure 4c,d). This quantity contains information on the near-field intensity distribution and is therefore related to the EEL probability maps,[31,32] as confirmed by the good agreement with the experimental results.

Examining the EEL spectra in Figure 4 obtained at different positions we observe that the dipolar edge plasmon (mode 1) is

DOI: 10.1021/acsphotonics.5b00594
ACS Photonics 2016, 3, 428−433

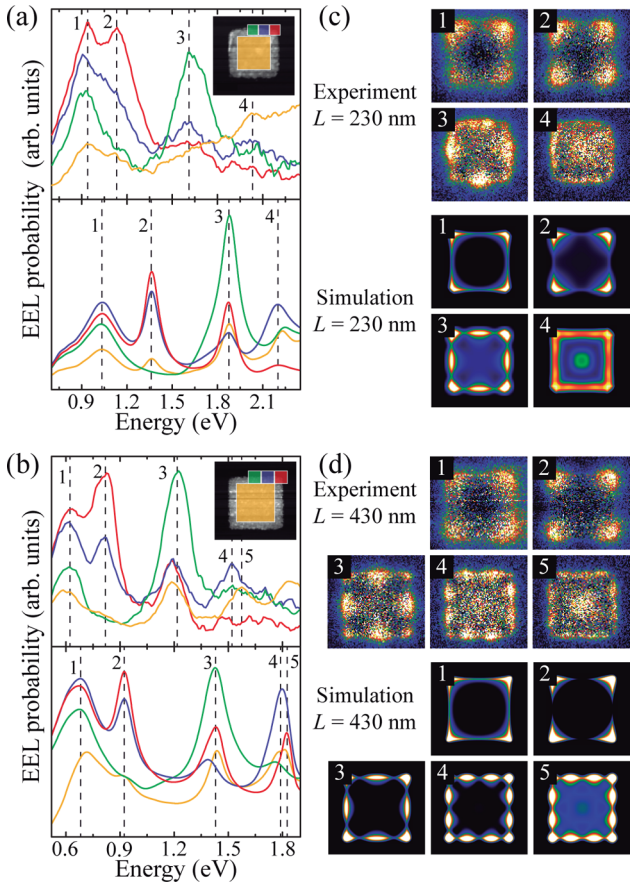

Figure 4. Comparison between EEL measurements and theoretical simulations. (a,b) Experimental (top) and simulated (bottom) EEL spectra for silver nanosquares of L = 230 nm and L = 430 nm. (c,d) Experimental EEL maps (top) and simulated LDOS maps (bottom) for the different plasmon modes shown in (a) and (b).

more homogeneously distributed along the edge of the nanosquare than the quadrupolar edge plasmon (mode 2). This is seen from the faster decay of the EEL intensity associated with the latter as we move away from the corner (cf. red, blue, and green curves in Figures 4a,b) and is consistent with our previous analysis based on the number of nodes along the edge. In a similar way, mode 3 has a strong peak at the center of the edge, as expected from the number of nodes associated with this mode. However, the measured EEL probability at the corner is smaller than what is predicted theoretically, something that we attribute to the departure of the fabricated nanostructure from a perfect square shape. The theoretical simulations also demonstrate the formation of the cavity plasmon modes, as seen from the increase of the relative intensity of the EEL spectra at the center of the nanostructure (yellow curves), which is also corroborated by the simulated LDOS maps (cf. mode 4 in Figure 4c and mode 5 in Figure 4d). Again, the higher intensity at the edges in the simulated results as compared with the experimental data can be attributed to imperfections on the experimental geometry.

COMPARISON WITH SCATTERING CROSS-SECTION

We can complete the characterization of the plasmonic response of the silver nanosquares by performing a theoretical simulation of their optical scattering cross-sections. Such comparison allows us to highlight the power of EELS to resolve both spatially and spectrally high multipolar modes. The results of the calculation of the scattering cross-section for normal incidence are shown in Figure 5 (gray curves) along

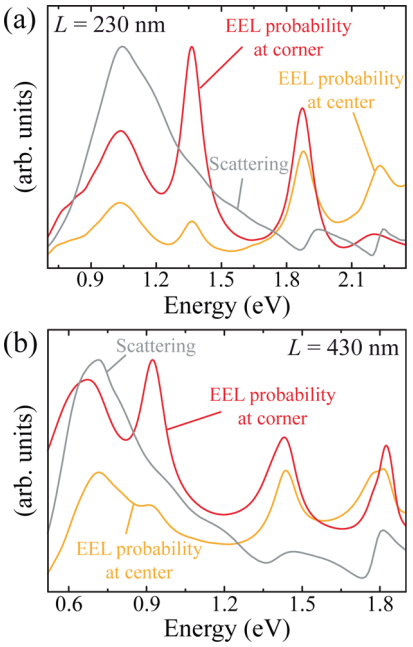

Figure 5. Comparison between EEL and optical spectra. We consider silver nanosquares with lateral size L = 230 nm (a) and L = 430 nm (b). The gray curves correspond to the optical scattering cross-section of the silver nanosquares calculated at normal incidence, while the EEL spectra are computed for electron trajectories passing through the center (yellow curves) and the corner (red curves) of the nanostructure.

with the EEL spectra obtained for electron beam trajectories passing through the center (yellow curves) and the corner (red curves) of the nanostructure. Interestingly, the scattering spectrum only shows one large peak, which corresponds to the dipolar edge plasmon supported by the nanosquares. The reason is that higher multipolar modes couple more weakly to light than the dipolar mode and because of that are commonly known as dark modes.[33,34] This is the case of the quadrupolar edge plasmon, which is clearly visible in the EEL spectra but does not show up in the optical spectrum. It is important to notice that the large size of the nanostructures studied here makes possible the excitation of the dark modes using tilted illumination thanks to the symmetry-breaking caused by retardation.[35] This is shown in Figure S3 of the Supporting Information, where we compare the cross-section calculated for light impinging at normal and 45° incidence. Interestingly, the next two modes appear in the scattering spectra in the form of weak Fano resonances.[36,37] These resonances are the result of the interaction between a bright superradiant mode with a broad line shape and a dark subradiant mode displaying a narrow line shape. In our particular case, the dipolar edge plasmon acts as the bright mode, while the dark modes are the higher multipolar modes (cf. modes 3 and 4 in Figure 4). The interaction between these modes is facilitated by symmetry-breaking provided by the presence of the substrate and retardation. Dark modes, due to their reduced radiative losses, have significantly narrower lineshapes than bright modes. This fact can be used, for instance, to improve the efficiency of

DOI: 10.1021/acsphotonics.5b00594
ACS Photonics 2016, 3, 428−433

plasmon induced hot carrier generation.[38,39] However, any application exploiting these modes requires an exquisite level of characterization of the spatial and the spectral response of the nanostructure such as the one demonstrated here using EELS.

CONCLUSIONS

In summary, we have used EELS and rigorous modeling to characterize the plasmonic response of silver nanosquares of several sizes supported by silicon nitride substrates. We have found that these nanostructures support a collection of multipolar edge and cavity modes, whose nature we have investigated through the analysis of the corresponding EEL probability maps. The characterization of these modes, which have not been previously detected in smaller structures, has only been possible by pushing the detection to the current limits of this technique. Furthermore, by comparing the EEL spectra with optical scattering cross-section calculations, we have confirmed that most the modes supported by the nanosquares are dark and cannot be detected using optical measurements due to their high multipolar nature. The results emphasize, yet again, the well-established versatility of EELS and the sensitivity of this technique to probe both bright and dark plasmon resonances. By analyzing a range of simple structures, we have shown that the combination of EELS experiments and theory provides fundamental understanding of the plasmon physics necessary to improve the design and optimization of new nanostructures for nanophotonic applications.

ASSOCIATED CONTENT

Supporting Information

The Supporting Information is available free of charge on the ACS Publications website at DOI: 10.1021/acsphotonics.5b00594.

Additional EEL probability maps similar to those shown in Figure 2c,d for nanosquares with lateral sizes L = 640 nm and L = 1 μm, a theoretical study of the effect of the substrate thickness t and refractive index n (see Figure 1) on the EEL spectra of the silver nanosquares, and a comparison of the scattering cross-section for normal and 45° incidence (PDF)

Movie showing the evolution of the EEL probability maps for the square with L = 850 nm as a function of energy (range 1−1.9 eV), which was generated by filtering the acquired data with the smoothing filter in Matlab using a "box" convolution kernel of size [5, 5, 7] (AVI)

AUTHOR INFORMATION

Corresponding Authors

*For P.N.: E-mail, nordland@rice.edu.

*For G.A.B.: E-mail, gbotton@mcmaster.ca.

Notes

The authors declare no competing financial interest.

ACKNOWLEDGMENTS

E.P.B. is grateful to McMaster University for financial support through the International Excellence Scholarship and the Ontario Graduate Scholarship. E.B.P. and G.A.B. acknowledge support from NSERC under the Discovery Grant Program. A.M. acknowledges financial support from the Department of Physics and Astronomy and the College of Arts and Sciences of the University of New Mexico. P.N. acknowledges support from the Robert A. Welch Foundation under grant C-1222 and the Army Research Office MURI grant WF911NF-12-0407. The Experimental work was carried out at the Canadian Centre for Electron Microscopy, a National Facility supported by NSERC, The Canada Foundation for Innovation (the MSI program), and McMaster University.

REFERENCES

(1) Maier, S. A. *Plasmonics: Fundamentals and Applications*; Springer: New York, 2007.

(2) Halas, N. J.; Lal, S.; Chang, W.; Link, S.; Nordlander, P. Plasmons in strongly coupled metallic nanostructures. *Chem. Rev.* **2011**, *111*, 3913−3961.

(3) Novotny, L.; Hecht, B. *Principles of Nano-Optics*; Cambridge University Press: New York, 2006.

(4) Betzig, E.; Finn, P. L.; Weiner, J. S. Combined shear force and near-field scanning optical microscopy. *Appl. Phys. Lett.* **1992**, *60*, 2484−2486.

(5) Hartschuh, A. Tip-enhanced near-field optical microscopy. *Angew. Chem., Int. Ed.* **2008**, *47*, 8178−8191.

(6) García de Abajo, F. J. Optical excitations in electron microscopy. *Rev. Mod. Phys.* **2010**, *82*, 209−275.

(7) Kociak, M.; Stephan, O. Mapping plasmons at the nanometer scale in an electron microscope. *Chem. Soc. Rev.* **2014**, *43*, 3865−3883.

(8) Nelayah, J.; Kociak, M.; Stéphan, O.; García de Abajo, F. J.; Tencé, M.; Henrard, L.; Taverna, D.; Pastoriza-Santos, I.; Liz-Marzán, L. M.; Colliex, C. Mapping surface plasmons on a single metallic nanoparticle. *Nat. Phys.* **2007**, *3*, 348−353.

(9) Egerton, R. F. Limits to the spatial, energy and momentum resolution of electron energy-loss spectroscopy. *Ultramicroscopy* **2007**, *107*, 575−586.

(10) Schaffer, B.; Hohenester, U.; Trügler, A.; Hofer, F. High-resolution surface plasmon imaging of gold nanoparticles by energy-filtered transmission electron microscopy. *Phys. Rev. B: Condens. Matter Mater. Phys.* **2009**, *79*, 041401(R).

(11) Nelayah, J.; Gu, L.; Sigle, W.; Koch, C. T.; Pastoriza-Santos, I.; Liz-Marzán, L. M.; van Aken, P. A. Direct imaging of surface plasmon resonances on single triangular silver nanoprisms at optical wavelength using low-loss EFTEM imaging. *Opt. Lett.* **2009**, *34*, 1003−1005.

(12) Nicoletti, O.; Wubs, M.; Mortensen, N. A.; Sigle, W.; van Aken, P. A.; Midgley, P. A. Surface plasmon modes of a single silver nanorod: an electron energy loss study. *Opt. Express* **2011**, *19*, 15371−15379.

(13) Zhu, G.; Radtke, G.; Botton, G. A. Bonding and structure of a reconstructed (001) surface of SrTiO3 from TEM. *Nature* **2012**, *490*, 384−387.

(14) Myroshnychenko, V.; Nelayah, J.; Adamo, G.; Geuquet, N.; Rodríguez-Fernández, J.; Pastoriza-Santos, I.; MacDonald, K. F.; Henrard, L.; Liz-Marzán, L. M.; Zheludev, N. I.; Kociak, M.; García de Abajo, F. J. Plasmon spectroscopy and imaging of individual gold nanodecahedra: a combined optical microscopy, cathodoluminescence, and electron energy-loss spectroscopy study. *Nano Lett.* **2012**, *12*, 4172−4180.

(15) Duan, H.; Fernández-Domí-nguez, A. I.; Bosman, M.; Maier, S. A.; Yang, J. K. W. Nanoplasmonics: classical down to the nanometer scale. *Nano Lett.* **2012**, *12*, 1683−1689.

(16) Koh, A. L.; Bao, K.; Khan, I.; Smith, W. E.; Kothleitner, G.; Nordlander, P.; Maier, S. A.; McComb, D. W. Electron energy-loss spectroscopy (EELS) of surface plasmons in single silver nanoparticles and dimers: Influence of beam damage and mapping of dark modes. *ACS Nano* **2009**, *3*, 3015−3022.

(17) Rossouw, D.; Couillard, M.; Vickery, J.; Kumacheva, E.; Botton, G. A. Multipolar plasmonic resonances in silver nanowire antennas imaged with a subnanometer electron probe. *Nano Lett.* **2011**, *11*, 1499−1504.

(18) Liang, H.; Zhao, H.; Rossouw, D.; Wang, W.; Xu, H.; Botton, G. A.; Ma, D. Silver nanorice structures: oriented attachment-dominated

DOI: 10.1021/acsphotonics.5b00594
ACS Photonics 2016, 3, 428−433

growth, high environmental sensitivity, and real-space visualization of multipolar resonances. *Chem. Mater.* **2012**, *24*, 2339−2346.
(19) Diaz-Egea, C.; Sigle, W.; van Aken, P. A.; Molina, S. High spatial resolution mapping of surface plasmon resonance modes in single and aggregated gold nanoparticles assembled on DNA strands. *Nanoscale Res. Lett.* **2013**, *8*, 337.
(20) Barrow, S. J.; Rossouw, D.; Funston, A. M.; Botton, G. A.; Mulvaney, P. Mapping bright and dark modes in gold nanoparticle chains using electron energy loss spectroscopy. *Nano Lett.* **2014**, *14*, 3799−3808.
(21) Martin, J.; Kociak, M.; Mahfoud, Z.; Proust, J.; Gérard, D.; Plain, J. High-resolution imaging and spectroscopy of multipolar plasmonic resonances in aluminum nanoantennas. *Nano Lett.* **2014**, *14*, 5517−5523.
(22) Bellido, E. P.; Rossouw, D.; Botton, G. A. Toward 10 meV electron energy-loss spectroscopy resolution for plasmonics. *Microsc. Microanal.* **2014**, *20*, 767−778.
(23) Rossouw, D.; Botton, G. A. Plasmonic Response of Bent Silver Nanowires for Nanophotonic Subwavelength Waveguiding. *Phys. Rev. Lett.* **2013**, *110*, 066801.
(24) Guillaume, S.-O.; García de Abajo, F. J.; Henrard, L. Efficient modal-expansion discrete-dipole approximation: Application to the simulation of optical extinction and electron energy-loss spectroscopies. *Phys. Rev. B: Condens. Matter Mater. Phys.* **2013**, *88*, 245439.
(25) Schmidt, F.-P.; Ditlbacher, H.; Hohenester, U.; Hohenau, A.; Hofer, F.; Krenn, J. R. Dark plasmonic breathing modes in silver nanodisks. *Nano Lett.* **2012**, *12*, 5780−5783.
(26) Gu, L.; Sigle, W.; Koch, C. T.; Ögüt, B.; van Aken, P. A.; Talebi, N.; Vogelgesang, R.; Mu, J.; Wen, X.; Mao, J. Resonant wedge-plasmon modes in single-crystalline gold nanoplatelets. *Phys. Rev. B: Condens. Matter Mater. Phys.* **2011**, *83*, 195433.
(27) Goris, B.; Guzzinati, G.; Fernández-López, C.; Pérez-Juste, J.; Liz-Marzán, L. M.; Trügler, A.; Hohenester, U.; Verbeeck, J.; Bals, S.; Van Tendeloo, G. V. Plasmon mapping in Au@Ag nanocube assemblies. *J. Phys. Chem. C* **2014**, *118*, 15356−15362.
(28) Schmidt, F.-P.; Ditlbacher, H.; Hohenester, U.; Hohenau, A.; Hofer, F.; Krenn, J. Universal dispersion of surface plasmons in flat nanostructures. *Nat. Commun.* **2014**, *5*, 3604.
(29) Zhu, X. L.; Ma, Y.; Zhang, J. S.; Xu, J.; Wu, X. F.; Zhang, Y.; Han, X. B.; Fu, Q.; Liao, Z. M.; Chen, L.; Yu, D. P. Confined three-dimensional plasmon modes inside a ring-shaped nanocavity on a silver film imaged by cathodoluminescence microscopy. *Phys. Rev. Lett.* **2010**, *105*, 127402.
(30) Cao, Y.; Manjavacas, A.; Large, N.; Nordlander, P. Electron Energy-Loss Spectroscopy Calculation in Finite-Difference Time-Domain Package. *ACS Photonics* **2015**, *2*, 369−375.
(31) García de Abajo, F. J.; Kociak, M. Probing the photonic local density of states with electron energy loss spectroscopy. *Phys. Rev. Lett.* **2008**, *100*, 106804.
(32) Hohenester, U.; Ditlbacher, H.; Krenn, J. R. Electron-energy-loss spectra of plasmonic nanoparticles. *Phys. Rev. Lett.* **2009**, *103*, 106801.
(33) Ögüt, B.; Talebi, N.; Vogelgesang, R.; Sigle, W.; van Aken, P. A. Toroidal Plasmonic Eigenmodes in Oligomer Nanocavities for the Visible. *Nano Lett.* **2012**, *12*, 5239−5244.
(34) Losquin, A.; Zagonel, L. F.; Myroshnychenko, V.; Rodrí-guez-González, B.; Tencé, M.; Scarabelli, L.; Förstner, J.; Liz-Marzán, L. M.; García de Abajo, F. J.; Stéphan, O.; Kociak, M. Unveiling nanometer scale extinction and scattering phenomena through combined electron energy loss spectroscopy and cathodoluminescence measurements. *Nano Lett.* **2015**, *15*, 1229−1237.
(35) Krug, M. K.; Reisecker, M.; Hohenau, A.; Ditlbacher, H.; Trügler, A.; Hohenester, U.; Krenn, J. R. Probing plasmonic breathing modes optically. *Appl. Phys. Lett.* **2014**, *105*, 171103.
(36) Fano, U. Effects of configuration interaction on intensities and phase shifts. *Phys. Rev.* **1961**, *124*, 1866−1878.
(37) Luk'yanchuk, B.; Zheludev, N. I.; Maier, S. A.; Halas, N. J.; Nordlander, P.; Giessen, H.; Chong, C. The Fano resonance in plasmonic nanostructures and metamaterials. *Nat. Mater.* **2010**, *9*, 707−715.
(38) Fang, Z.; Liu, Z.; Wang, Y.; Ajayan, P. M.; Nordlander, P.; Halas, N. J. Graphene-antenna sandwich photodetector. *Nano Lett.* **2012**, *12*, 3808−3813.
(39) Brongersma, M. L.; Halas, N. J.; Nordlander, P. Plasmon-induced hot carrier science and technology. *Nat. Nanotechnol.* **2015**, *10*, 25−34.

DOI: 10.1021/acsphotonics.5b00594
ACS Photonics 2016, 3, 428−433